BRAIN
A JOURNAL OF NEUROLOGY

Serotonergic signalling suppresses ataxin 3 aggregation and neurotoxicity in animal models of Machado-Joseph disease

Andreia Teixeira-Castro,[1,2,3,4,]* Ana Jalles,[1,2,]* Sofia Esteves,[1,2,]* Soosung Kang,[3,5,6] Liliana da Silva Santos,[1,2] Anabela Silva-Fernandes,[1,2] Mário F. Neto,[3,4] Renée M. Brielmann,[3,4] Carlos Bessa,[1,2] Sara Duarte-Silva,[1,2] Adriana Miranda,[1,2] Stéphanie Oliveira,[1,2] Andreia Neves-Carvalho,[1,2] João Bessa,[1,2] Teresa Summavielle,[7] Richard B. Silverman,[3,5,6] Pedro Oliveira,[8] Richard I. Morimoto[3,4] and Patrícia Maciel[1,2]

*These authors contributed equally to this work.

Polyglutamine diseases are a class of dominantly inherited neurodegenerative disorders for which there is no effective treatment. Here we provide evidence that activation of serotonergic signalling is beneficial in animal models of Machado-Joseph disease. We identified citalopram, a selective serotonin reuptake inhibitor, in a small molecule screen of FDA-approved drugs that rescued neuronal dysfunction and reduced aggregation using a *Caenorhabditis elegans* model of mutant ataxin 3-induced neurotoxicity. MOD-5, the *C. elegans* orthologue of the serotonin transporter and cellular target of citalopram, and the serotonin receptors SER-1 and SER-4 were strong genetic modifiers of ataxin 3 neurotoxicity and necessary for therapeutic efficacy. Moreover, chronic treatment of CMVMJD135 mice with citalopram significantly reduced ataxin 3 neuronal inclusions and astrogliosis, rescued diminished body weight and strikingly ameliorated motor symptoms. These results suggest that small molecule modulation of serotonergic signalling represents a promising therapeutic target for Machado-Joseph disease.

1 Life and Health Sciences Research Institute (ICVS), School of Health Sciences, University of Minho, 4710-057 Braga, Portugal
2 ICVS/3Bs - PT Government Associate Laboratory, Braga/Guimarães, Portugal
3 Department of Molecular Biosciences, Northwestern University, Evanston, Illinois 60208, USA
4 Rice Institute for Biomedical Research, Northwestern University, Evanston, Illinois 60208, USA
5 Department of Chemistry, Northwestern University, Evanston, Illinois 60208, USA
6 Chemistry of Life Processes Institute and Center for Molecular Innovation and Drug Discovery, Northwestern University, Evanston, Illinois 60208, USA
7 IBMC - Instituto de Biologia Molecular e Celular, Universidade do Porto, Rua do Campo Alegre, 823, 4150-180 Porto, Portugal
8 ICBAS-Abel Salazar Biomedical Sciences Institute, University of Porto, Porto, Portugal

Correspondence to: Patrícia Maciel, PhD
Life and Health Sciences Research Institute (ICVS);
School of Health Sciences; University of Minho;
Gualtar Campus, 4710-057 Braga,
Portugal
E-mail: pmaciel@ecsaude.uminho.pt

Introduction

The expansion of trinucleotide CAG repeats causes hereditary adult-onset neurodegenerative disorders such as Huntington's disease, spinobulbar muscular atrophy, dentatorubral-pallidoluysian atrophy and six forms of spinocerebellar ataxia (Ross *et al.*, 1998). Machado-Joseph disease (or spinocerebellar ataxia type 3, SCA3), the most common dominantly inherited SCA worldwide (Schols *et al.*, 2004), is characterized by ataxia, ophthalmoplegia and pyramidal signs, associated with dystonia, spasticity, peripheral neuropathy and amyotrophy (Coutinho and Andrade, 1978), without cognitive decline. Pathologically, there is degeneration of the deep nuclei of the cerebellum, pontine and subthalamic nuclei, substantia nigra and spinocerebellar nuclei. The genetic basis of Machado-Joseph disease is the expansion of a polyglutamine tract within the protein ataxin 3 (ATXN3) (Kawaguchi *et al.*, 1994). When the polyglutamine tract exceeds 60 consecutive glutamines, ATXN3 becomes highly aggregation prone, leading to an imbalance in cellular proteostasis, as aggregation-associated proteotoxicity dominates over folding and clearance (Balch *et al.*, 2008; Morimoto, 2008).

Currently there is no treatment for Machado-Joseph disease that effectively slows disease progression. Efforts to improve patient quality of life and to sustain independence address the restless legs and extrapyramidal syndromes, treatment of cramps and of the effects of fatigue (D'Abreu *et al.*, 2010). Not yet translated to clinical practice are therapeutic strategies that include the use of small molecules or gene targeting to manipulate the concentration, conformation, and/or location of ATXN3. For example, it is known that modulating the levels of molecular chaperones Hsp70, alphaB-crystallin and Hsp104 could prevent or inhibit ATXN3 aggregation, and promote its disaggregation (Warrick *et al.*, 2005; Robertson *et al.*, 2010; Cushman-Nick *et al.*, 2013). Treatment with Hsp90 inhibitors that increase chaperone expression had beneficial effects, although it failed to achieve the predicted molecular effect of chaperone induction in animal models of Machado-Joseph disease (Silva-Fernandes *et al.*, 2014). Likewise, activation of autophagy, either genetic or pharmacological, lessened ATXN3 pathogenesis *in vivo* (Menzies *et al.*, 2010; Nascimento-Ferreira *et al.*, 2013). In rodents, reversion of the expanded polyglutamine-associated transcription downregulation by a histone deacetylase (HDAC) inhibitor rescued ataxic symptoms (Chou *et al.*, 2011). Dantrolene administration (targeting intracellular calcium homeostasis) improved motor performance and prevented neuronal loss (Chen *et al.*, 2008). While silencing of *ATXN3* offers potential, the impact of this type of treatment to date has not been promising in Machado-Joseph disease mice (Costa Mdo *et al.*, 2013; Nobrega *et al.*, 2013). For many proposed therapies, translation into clinical practice will be further limited by human safety. The traditional approach to drug discovery, which involves *de novo* identification and validation of new molecular targets, is costly and time-consuming, thus limiting the number of new drugs introduced into the clinic (Shim and Liu, 2014). Moreover, as the average time required for drug development continues to increase, there has been renewed interest in drug repurposing strategies (Chong and Sullivan, 2007; Shim and Liu, 2014). On the other hand, in past years, the primary cause of new drug candidate failures has been low therapeutic efficacy in clinical trials. Among the most frequently proposed reasons for this shortcoming is the lack of translation of *in vitro* and recombinant drug activity to therapeutic *in vivo* whole organism systems. As an approach to identify novel therapeutic strategies, we used *Caenorhabditis elegans* (*C. elegans*), a powerful platform to model neurodegenerative disease and for characterization of small bioactive molecules (Kaletta and Hengartner, 2006). Previously, we established a *C. elegans* model for Machado-Joseph disease pathogenesis in which expression of mutant ATXN3 in the nervous system led to its progressive aggregation in distinct neuronal subtypes and altered motor behaviour (Teixeira-Castro *et al.*, 2011a). Here, we used this model to screen a library of FDA-approved small molecules, and identified compounds that rescued or ameliorated mutant ATXN3-mediated neurological dysfunction. By combining compound treatment with genetic tools, we demonstrate that modulation of serotonergic signalling by selective serotonin reuptake inhibitors (SSRIs) suppressed mutant ATXN3 aggregation and neurotoxicity in both *C. elegans* and mice. This reveals the utility of the approach by which safe and highly effective bioactive small molecules can be repurposed to benefit rare diseases lacking effective therapies. The finding that serotonin recapture inhibition modulates proteotoxicity may be relevant for other protein conformation disorders.

Materials and methods

Study design

The overall objective of the study was to find novel therapeutic targets for Machado-Joseph disease. The first part of this study was designed to identify novel suppressor compounds of mutant ATXN3 pathogenesis *in vivo*, using a hypothesis-free approach. The second aim of the study was to validate one of the identified drugs in a vertebrate model of the disease. To achieve the two goals, a small molecule screening of a FDA-approved library was conducted using a transgenic *C. elegans* model of the disease (Teixeira-Castro *et al.*, 2011a). The most promising hit of the screening regarding human safety, target specificity and conservation across evolution was tested in CMVMJD135 mice (Silva-Fernandes *et al.*, 2014). For all animal experiments, we ensured blinded outcome assessment. Experimental design was based on power analyses for optimization of sample size. *C. elegans* (Supplementary Table 1) and mice (Supplementary Table 2) sample size calculations were performed for each behavioural test and pathological analyses assuming a power of 0.95 and 0.8, respectively, and a significance level of $P < 0.05$. The effect size was calculated aiming for a 50% improvement. In general, we used $n = 3–4$

per genotype/treatment of *C. elegans* for motility assays, $n = 8$–14 for aggregation (with three replicates) and $n = 4$ for immunoblotting. For mice, we used $n = 13$–16 per genotype/treatment for behavioural tests, and a group size of four animals per group for quantification of ATXN3 intranuclear inclusions, assessment of astrogliosis and western blot analysis. All experiments were designed with commitment to the principles of refinement, reduction, and replacement and performed according to the FELASA guidelines to minimize discomfort, stress, and pain to the animals, with defined humane endpoints (1994).

Nematode strains and general methods

For a list of strains used in this work and abbreviations, see Supplementary Table 3. All the strains were backcrossed to Bristol strain N2 five to eight times. Standard methods were used for culturing and observing *C. elegans*, unless otherwise noted (Brenner, 1974). Nematodes were grown on nematode growth medium plates seeded with *Escherichia coli* OP50 strain at 20°C.

Compounds

All the compounds were obtained from the commercial vendors indicated below and were used without further purification. The Prestwick Chemical Library™ (Prestwick Chemical) used for the *C. elegans* screening comprised 1120 chemical and pharmacologically diverse small molecules. Other compounds used, including the 11 hits selected for validation, were reordered from a different manufacturer before repetition of experiments: 17-(allylamino)-17-demethoxygeldanamycin (17-AAG) CAS 75747-14-7 (Biomol); nisoxetine hydrochloride CAS 57754-86-6 (Sigma); scoulerine CAS 6451-73-6 (Toronto Research); eburnamonine CAS 4880-88-0 (Santa Cruz); piperlongumine CAS 20069-09-4 (Biotrend); chlortetracycline hydrochloride CAS 64-72-2 (Sigma); tiapride hydrochloride CAS 51012-33-0 (Sigma); clemizole hydrochloride CAS 1163-36-6 (Sigma); metixene hydrochloride CAS 7081-40-5 (Sigma); budesonide CAS 51333-22-3 (Sigma); noscapine CAS 128-62-1 (Sigma); estrone CAS 53-16-7 (Sigma); fluoxetine CAS 56296-78-7 (Kemprotec Ltd.); zimelidine CAS 61129-30-4 (Sigma); lyzergol CAS 602-85-7 (Sigma); pindolol CAS 13523-86-9 (Sigma); trazodone hydrochloride CAS 25332-39-2 (Sigma); citalopram hydrobromide CAS 59729-32-7 (Kemprotec Ltd.); escitalopram (S-citalopram) hydrobromide CAS 219861-08-2 (Kemprotec Ltd). Citalopram used for studies in mice and vabicaserin were kindly provided by Lündbeck.

Drug toxicity assay

Bristol strain N2 was used to screen the Prestwick Chemical Library™ for compound toxicity. The assay was performed in 96-well plate format, in liquid culture (Voisine *et al.*, 2007). Each well contained a final volume of 60 μl, comprising 20–25 animals in egg stage, drug at the appropriate concentration and OP50 bacteria to a final OD_{595} of 0.6–0.8 measured in the microplate reader (Bio-Rad microplate reader 680). To obtain the age synchronized population of eggs, gravid adults were treated with alkaline hypochlorite solution (0.5 M NaOH, ~2.6% NaClO)

for 7 min. The animals were then washed in M9 buffer, resuspended in S-medium to the appropriate egg number and transferred into the 96-well plate. The OP50 bacteria were grown overnight at 37°C and 150 rpm in Luria Broth (LB) media, pelleted by centrifugation, inactivated by four to six cycles of freeze/thawing, frozen at −80°C and then resuspended in S-medium supplemented with cholesterol, streptomycin, penicillin and nystatin (Sigma). Worms were grown with continuous shaking at 180 rpm at 20°C (Shel Lab) for 7 days. The compound library was prepared in 100% dimethyl sulphoxide (DMSO, Sigma) and tested at dilutions corresponding to a maximum concentration of 1% DMSO to avoid solvent-specific developmental defects and toxicity. For each compound, two final concentrations were tested (50 μM and 25 μM). The effect of compounds on *C. elegans* physiology was monitored by the rate at which the *E. coli* food suspension was consumed, as a read out for *C. elegans* growth, survival or fecundity. The absorbance (OD_{595}) was measured daily. OP50-only (S-medium, no vehicle), DMSO 1% (vehicle) and DMSO 5% (toxic condition) controls were used.

C. elegans assays for motility defects and aggregation

Wild-type (WT, N2), wild-type ATXN3 (AT3WT) and mutant ATXN3 (AT3q130) animals were grown in liquid culture in a 96-well plate format, with the chemical compounds, as described above. Four-day-old animals were transferred from the 96-well plates onto an unseeded nematode growth medium plate (equilibrated at 20°C). Plates were allowed to dry for 1 h before starting the assays. Motility assays were performed at 20°C as previously described (Gidalevitz *et al.*, 2006; Teixeira-Castro *et al.*, 2011a). Motor behaviour assays were run in triplicates or quadruplicates ($n = 3$ or 4), with a total of at least 150 animals tested per genotype and/or compound. For confocal dynamic imaging and quantification of ATXN3 aggregation, live animals were immobilized with 3 mM levamisole (Sigma) and mounted on a 3% agarose pad. All images were captured on an Olympus FV1000 (Japan) or Zeiss LSM 510 (Germany) confocal microscopes, under a ×60 oil (NA = 1.35) or ×63 water (NA = 1.0) objectives. Z-series imaging was acquired for all vehicle- and compound-treated animals, using a 515/514 nm laser excitation line for yellow fluorescent protein fusion proteins. The pinhole was adjusted to 1.0 Airy unit of optical slice, and a scan was acquired every ~0.5 μm along the z-axis. The quantification of the aggregates was performed as previously described (Teixeira-Castro *et al.*, 2011a, b). Three parameters were measured: area of aggregates/total area; number of aggregates/total area; and number of aggregates. Values shown are the mean (normalized to vehicle treated control) of eight or more animals per group, unless noted otherwise.

Chemical and pharmacological classification of the hits

Hits were manually inspected to categorize them into chemical and pharmacological classes based on MeSH tree (Medical Subject Headings; PubMed), ChEBI Ontology (Chemical Entities of Biological Interest), and ATC (Anatomical Therapeutic Chemical) fourth level classifications. The majority of the hits were sorted into heterocyclic, alkaloid, steroid,

polycyclic, and β-amino alcohol chemical classes, and further classified into neurotransmitter, anti-infective, cardiovascular, anti-inflammatory, analgesic, and hormone pharmacological classes. For a drug that has multiple therapeutic applications, all classes were equally considered. However, if a new multi-therapeutic drug shares the same structural and pharmacological class with a high scored single therapeutic compound, we considered only a single therapeutic application and clustered the new molecule into the same class. This classification allowed us simple observation of the chemical and pharmacological classes of the hits.

C. elegans citalopram time course assays

For time course experiments, animals were grown on nematode growth medium plates with OP50 supplemented with citalopram. OP50 cultures were prepared as described above and concentrated $10\times$ with S-media supplemented with streptomycin, penicillin and nystatin (Sigma). Stock solutions of citalopram (2.5 mM and 0.5 mM) (Kemprotec) or vehicle (DMSO) were prepared and added to OP50 cultures to a final concentration of 25 μM or 5 μM. Plates were seeded with 200 μl of OP50-citalopram/vehicle and left at room temperature to dry for at least 3 days. Fresh plates were prepared two to three times a week to prevent drug degradation. OFF-drug effect was evaluated by treating the animals for 4 days and after that time animals were transferred to DMSO plates (vehicle), shown in Fig. 2D as AT3q130::cit OFF. During the reproductive period, animals were transferred into new fresh plates every day.

Immunoblotting analysis

For determination of the steady-state protein levels of ATXN3, the animals were incubated in liquid culture with the chemical compounds in a 96-well plate format as described above. Four-day-old animals were transferred from the liquid culture onto an unseeded nematode growth medium plate (equilibrated at 20°C). After 1 h of acclimation 25 individual young adult animals were picked, boiled for 15 min in sodium dodecyl sulphate (SDS) sample buffer (to destroy all the aggregates) and the resulting extracts resolved on a 10% SDS gel, as previously described (Gidalevitz *et al.*, 2009; Teixeira-Castro *et al.*, 2011). Immunoblots were probed with anti-ATXN3 mouse (1H9, MAB5360, Milipore; 1:1000 or 1:150) and anti-tubulin mouse antibodies (T5168, Sigma; 1:5000); and detected with horseradish peroxidase-coupled secondary antibodies (Bio-Rad) and chemiluminescence (ECL western-blotting detecting reagents, Amersham Pharmacia). Protein isolation from mouse brainstem tissue and western blot were performed as previously described (Silva-Fernandes *et al.*, 2010). The blots were blocked and incubated overnight at 4°C with the primary antibody rabbit anti-ataxin 3 serum (kindly provided by Dr Henry Paulson) (1:5000) and mouse anti-GAPDH (G8795, Sigma, 1:1000). As a loading control, mouse ataxin 3 and GAPDH were used. Western blot quantifications were performed using Chemidoc XRS Software with ImageLab Software (Bio-Rad) or ImageJ software (NIH), according to the manufacturer's instructions. ATXN3 fractionation assays were performed as previously described (Koch *et al.*, 2011), with the following modifications: AT3q130 animals were grown for 4 days in

nematode growth medium-citalopram/vehicle plates. Nematodes were collected and washed in M9 buffer, and resuspended in RIPA buffer [50 mM Tris, 150 mM NaCl, 0.2% Triton™ X-100, 25 mM EDTA, supplemented with complete protease inhibitor (Roche)] before shock freezing in liquid nitrogen. After three freeze-thawing cycles, the worm pellet was ground with a motorized pestle, and lysed on ice, in the presence of 0.025 U/ml benzonase (Sigma). The lysate was centrifuged at 1000 rpm for 1 min in a table-top centrifuge to pellet the carcasses (Nussbaum-Krammer *et al.*, 2013). Protein concentration was determined using Bradford assay (Bio-Rad) and was set to a final concentration of 3–4 μg/μl in all experimental conditions and followed by a 22 000 g centrifugation for 30 min at 4°C. The pellet fractions were separated from supernatants (Triton™ X-100-soluble fraction) and homogenized in 150 μl RIPA buffer containing 2% SDS followed by a second centrifugation step at room temperature. The supernatants (SDS-soluble fraction) were removed, and the remaining pellets were incubated for 16 h in 100% formic acid at 37°C. After formic acid evaporation at 37°C, the pellet was dissolved in 25 μl Laemmli buffer (SDS-insoluble fraction) followed by pH adjustment with 2 M Tris-base for SDS–polyacrylamide gel electrophoresis analysis. Gels were loaded with 50 μg of the Triton™ X-100 fraction, 40 μl of the SDS-soluble fraction and the complete SDS-insoluble fraction. Western blot analyses were performed as described above.

Lifespan

Assays were performed at 20°C as previously described (Morley and Morimoto, 2004). Approximately 100 hermaphrodites were cultured on each Petri dish and were transferred to fresh plates every day until the cessation of progeny production, and about every 1–3 days thereafter. Animals were scored as dead if they showed no spontaneous movement or response when prodded. Dead animals that displayed internally hatched progeny, extruded gonad or desiccation were excluded.

Transgenic mouse model and drug administration

CMVMJD135 mice were generated as described previously (Silva-Fernandes *et al.*, 2014). DNA extraction, animal genotyping and CAG repeat size analyses were performed as previously described (Silva-Fernandes *et al.*, 2010). The mean repeat size [± standard deviation (SD)] for all mice used was 130 ± 2. Age-matched and genetic background-matched wild-type animals were used as controls. Only male mice were used in this study. We administrated citalopram hydrobromide CAS 59729-32-7 (Lündbeck, Denmark) in the drinking water at two doses (8 and 13 mg/kg/day) that roughly equate to the high dosage range prescribed to human patients for depression (Cirrito *et al.*, 2011). Treatment was initiated at 5 weeks of age, one week before the expected onset of the first neurological symptoms. The trial was ended at 34 weeks of age, according to the humane endpoints established for the non-treated CMVMJD135 mice. All animal procedures were conducted in accordance with European regulations (European Union Directive 86/609/EEC). Animal facilities and the people directly involved in animal experiments (A.T.C., S.E., A.S.F., S.D.S.) were certified by the Portuguese regulatory

entity - Direcção Geral de Alimentação e Veterinária. All of the protocols performed were approved by the Animal Ethics Committee of the Life and Health Sciences Research Institute, University of Minho.

Neurochemical quantification

CMVMJD135 and wild-type male littermate mice ($n = 5$–8) were sacrificed at 24 weeks of age by decapitation, their brains were rapidly removed, snap frozen in liquid nitrogen and dissected. Serotonin (5-HT) and 5-hydroxyindoleacetic acid (5-HIAA) levels were measured in the substantia nigra, medulla oblongata and cerebellum by high performance liquid chromatography, combined with electrochemical detection (HPLC/EC), as described previously (Santos et al., 2010). Concentrations of neurotransmitters were calculated using standard curves and results were expressed in terms of 5-HT and metabolism content per amount of protein.

Behavioural assessment

Behavioural analysis was performed during the diurnal period in groups of five males per cage including CMVMJD135 hemizygous transgenic mice and wild-type littermates ($n = 13$–16 per genotype) treated with citalopram or with vehicle (water). All behavioural tests started in a presymptomatic stage (4 weeks) and were conducted until 30 or 34 weeks of age. Neurological tests and general health assessment were performed using the SHIRPA protocol, enriched with the hanging wire test. The dragging of the paws and the stride length were evaluated with footprint analysis. Motor behaviour was further assessed using the balance beam walk test (12-mm square and 17-mm round beams) and the motor swimming test. All behavioural tests were performed as previously described (Silva-Fernandes et al., 2014). Body weight was also registered for each evaluation time point.

Immunohistochemistry and quantification of neuronal inclusions

Thirty-four-week-old wild-type and CMVMJD135 littermate mice, vehicle- and citalopram-treated ($n = 4$ for each group) were deeply anaesthetized [a mixture of ketamine hydrochloride (150 mg/kg) plus medetomidine (0.3 mg/kg)] and transcardially perfused with phosphate-buffered saline (PBS) followed by 4% paraformaldehyde (Panreac). Brains were removed and post-fixed overnight in paraformaldehyde and embedded in paraffin. Slides with 4-μm thick paraffin sections were subjected to antigen retrieval and then incubated with mouse anti-ATXN3 (1H9, MAB5360, Millipore; 1:100), rabbit anti-GFAP (Dako Corporation; 1:1000) or rabbit anti- Calbindin D-28 K (AB1778, Millipore, 1:1000) antibodies, which were detected by incubation with a biotinylated anti-polyvalent antibody, followed by detection through biotin-streptavidin coupled to horseradish peroxidase and reaction with the DAB (3, 3′-diaminobenzidine) substrate (Lab Vision™ Ultra-Vision™ Detection kit, Thermo Scientific). The slides were counterstained with haematoxylin 25% according to standard procedures. Fifty-micrometre thick vibrotome spinal cord sections were incubated with goat Anti-Choline Acetyltransferase (ChAT, Millipore, 1:500) and stained according to

VECTASTAIN® ABC system (Vector Laboratories). Thirty-four-week-old wild-type and CMVMJD135 littermate mice, vehicle- and citalopram-treated ($n = 4$ for each group), were deeply anaesthetized as mentioned above, transcardially perfused with NaCl (0.9%) and the mouse brains embedded in O.C.T. and rapidly frozen in isopentane (Sigma, CAS#78-78-4) chilled in liquid nitrogen. Slides with 30-μm thick cryostat sections were incubated with anti-ChAT according to the Lab Vision™ Ultra-Vision™ Detection kit instructions. ATXN3 positive inclusions in the pontine nuclei, reticulotegmental nucleus of the pons, facial motor nucleus and lateral reticular nucleus; stained astrocytes (GFAP-positive) in the substantia nigra; Calbindin D-28 K positive neurons in the cerebellar cortex; ChAT-positive neurons in the facial motor nucleus and in the ventral horn of the lumbar spinal cord of either vehicle- or citalopram-treated animals ($n = 3$–4 for each condition, four slides per animal) were quantified and normalized for total area using the Olympus BX51 stereological microscope (Olympus) and the Visiopharma integrator system software (Visopharm) as previously described (Silva-Fernandes et al., 2014).

Statistical analysis

Data were analysed through the non-parametric Mann-Whitney U-test when variables were non-continuous or when a continuous variable did not present a normal distribution (Kolmogorov-Smirnov test, $P < 0.05$). Continuous variables with normal distributions and with homogeneity of variance (Levene's test) were analysed with repeated measures ANOVA for longitudinal multiple comparisons and one-way ANOVA or Student's t-test for paired comparisons, using Tukey or Bonferroni tests for post hoc comparisons. When these two latter assumptions were not valid, an appropriate data transformation (e.g. logarithmic) was applied, and the data were re-analysed (body weight, balance beam walk test and motor swimming test). When logarithmic data transformation did not reduce the heterogeneity of variances (hanging wire test), several mathematical models were applied. In this test, the best fit model was the logarithmic and the treatment differences were analysed according the R squares of the CMVMJD135 groups, with a normal residual distribution. Statistical analysis of C. elegans survival assays was performed using the log rank (Mantel-Cox) test. All statistical analyses were performed using SPSS 20.0/22.0 (SPSS Inc.) and G-Power 3.1.9.2 (University Kiel, Germany). A critical value for significance of $P < 0.05$ was used throughout the study.

Results

A whole animal screen identifies small molecules that ameliorate mutant ataxin 3-mediated neuronal dysfunction

To identify small bioactive molecules with therapeutic value for Machado-Joseph disease, we screened a commercially available compound library, composed mainly of FDA/EMA-approved drugs, using a C. elegans model of

Machado-Joseph disease pathogenesis (AT3q130) in which mutant ATXN3 expressed in neurons caused aggregation and motility defects (Teixeira-Castro *et al.*, 2011). The strategy, validation approach and compound safety assays are depicted in Supplementary Figs 1 and 2. In the primary screen we identified 48 compounds (Fig. 1A) that ameliorated mutant ATXN3-mediated locomotion defects, showing a percentage of effect to non-treated animals higher than 50% within a confidence interval of 95% (Supplementary Fig. 3A). The hit compounds were categorized into chemical and pharmacological classes based on MeSH tree, ChEBI Ontology, and ATC fourth level classifications. While the chemical structure classification of the hit compounds revealed marked heterogeneity, they were enriched for specific pharmacological activities, namely modulators of neurotransmission (adrenergic, serotonergic, cholinergic, dopaminergic and histaminergic), anti-infectious, cardiovascular, anti-inflammatory, analgesic and hormone-related actions (Supplementary Fig. 3B).

A representative compound for each pharmacological cluster (Table 1) was further assessed for safety (Supplementary Fig. 2B) and ability to ameliorate motility impairment of mutant ATXN3 animals (Fig. 1B). The motility of wild-type animals was not increased by any of these hit compounds, suggesting that their action is specifically targeting mutant ATXN3-mediated pathogenesis (data not shown). Next, we examined whether these compounds affected protein aggregation in neurons of AT3q130 animals *in vivo*, and showed that the majority also decreased mutant ATXN3 aggregation (Fig. 1C). The reduction in ATXN3 aggregation was not due to decreased steady state levels of ATXN3 protein, suggesting a mechanism more likely related to folding stability than enhanced clearance (Fig. 1D). In summary, this *C. elegans* AT3q130 repurposing screen identified compounds with novel activity as suppressors of ATXN3 pathogenesis.

Pharmacological and genetic inhibition of *C. elegans* SERT suppresses ATXN3 pathogenesis

Among the largest class of compounds that suppressed mutant ATXN3-mediated pathogenesis were those that affected serotonergic neurotransmission and modulated 5-HT-mediated signalling (Fig. 1E). Of these, citalopram is a SSRI with a proven safety record that is widely used for treatment of depression (Mandrioli *et al.*, 2012). The primary molecular target of citalopram is the 5-HT transporter (SERT, encoded by *SLC6A4*), which is responsible for 5-HT reuptake by serotonergic neurons (Blakely *et al.*, 1994). This target specificity and conservation prompted us to further examine the effects of citalopram on Machado-Joseph disease pathogenesis. Treatment with citalopram caused complete rescue of mutant ATXN3-mediated neuronal dysfunction (Fig. 1E), with a dose-response profile and a derived half-maximal effective concentration (EC_{50}) value of 1 μM (Supplementary

Fig. 4A). Citalopram exists as a racemic mixture but its effects are largely due to the S-enantiomer, escitalopram; this and other SSRIs also had beneficial effects on AT3q130 animals (Supplementary Fig. 4B). Normal behaviour and motility, development and fecundity in wild-type animals were not affected by SSRI treatment (Supplementary Fig. 4C). Importantly, citalopram treatment significantly reduced mutant ATXN3 aggregation in *C. elegans* neurons (Fig. 2A), and increased ATXN3 solubility (Fig. 2B), as assessed by biochemical fractionation (Koch *et al.*, 2011), without affecting the overall level of protein (Fig. 2C).

On continuous exposure to citalopram, the survival of AT3q130 animals was rescued (Supplementary Fig. 4D and E) and their neuronal dysfunction was restored through to Day 14 of age (Fig. 2D). This beneficial effect declined when citalopram was withdrawn, and neurotoxicity returned after 3-4 days OFF treatment (AT3q130::cit OFF, Fig. 2D). Maximum protection required early treatment (from the egg stage through to Day 4 of adulthood) (Fig. 2E); moreover, the extent of drug exposure period was critical, as 2 days of treatment were insufficient to exert beneficial effects (Fig. 2F).

In *C. elegans*, there is one 5-HT transporter orthologue of the vertebrate SERT, MOD-5 (Ranganathan *et al.*, 2001). To confirm the beneficial effect of pharmacological inhibition of serotonin recapture, we showed that genetic ablation of MOD-5 rescued mutant ATXN3-mediated motor dysfunction and aggregation in *C. elegans* (Fig. 2G). Pharmacogenetic analysis also supported MOD-5 as a cellular target of citalopram in the nematode, as drug treatment did not further ameliorate mutant ATXN3-mediated pathogenesis in the absence of MOD-5. In contrast, estrone (a steroid hormone) was able to further reduce the motility impairment of *mod-5*; AT3q130 animals (Fig. 2G), which is consistent with independent modes of action for these two compounds.

The role of 5-HT receptors was examined using pharmacological and pharmacogenetic approaches (Fig. 3A). Activation of postsynaptic 5-HT receptors by the 5-HT2C receptor (*HTR2C*) agonist vabicaserin (Dunlop *et al.*, 2011) and stimulation of the presynaptic 5-HT autoreceptors by buspirone (Takei *et al.*, 2005), dihydroergotamine (Villalon *et al.*, 2003) (Fig. 3B), lysergol (Pertz *et al.*, 1999) or pindolol (Corradetti *et al.*, 1998) (Fig. 1D) ameliorated mutant ATXN3-mediated motor dysfunction. Consistent with this, genetic ablation of the 5-HT postsynaptic G-protein coupled receptor SER-1 (Hamdan *et al.*, 1999) enhanced AT3q130 aggregation and locomotion defects (Fig. 3C). Likewise, the effect of citalopram was also dependent on these receptors. Additionally, ablation of the SER-4 (Olde and McCombie, 1997) autoreceptor, which by eliminating the negative feedback likely increases 5-HT availability, restored locomotion and reduced ATXN3 aggregation *in vivo* (Fig. 3D). Taken together, these results support the idea that pharmacological and genetic inhibition of MOD-5 restores motility and suppresses aggregation of AT3q130 through modulation of 5HTR activity.
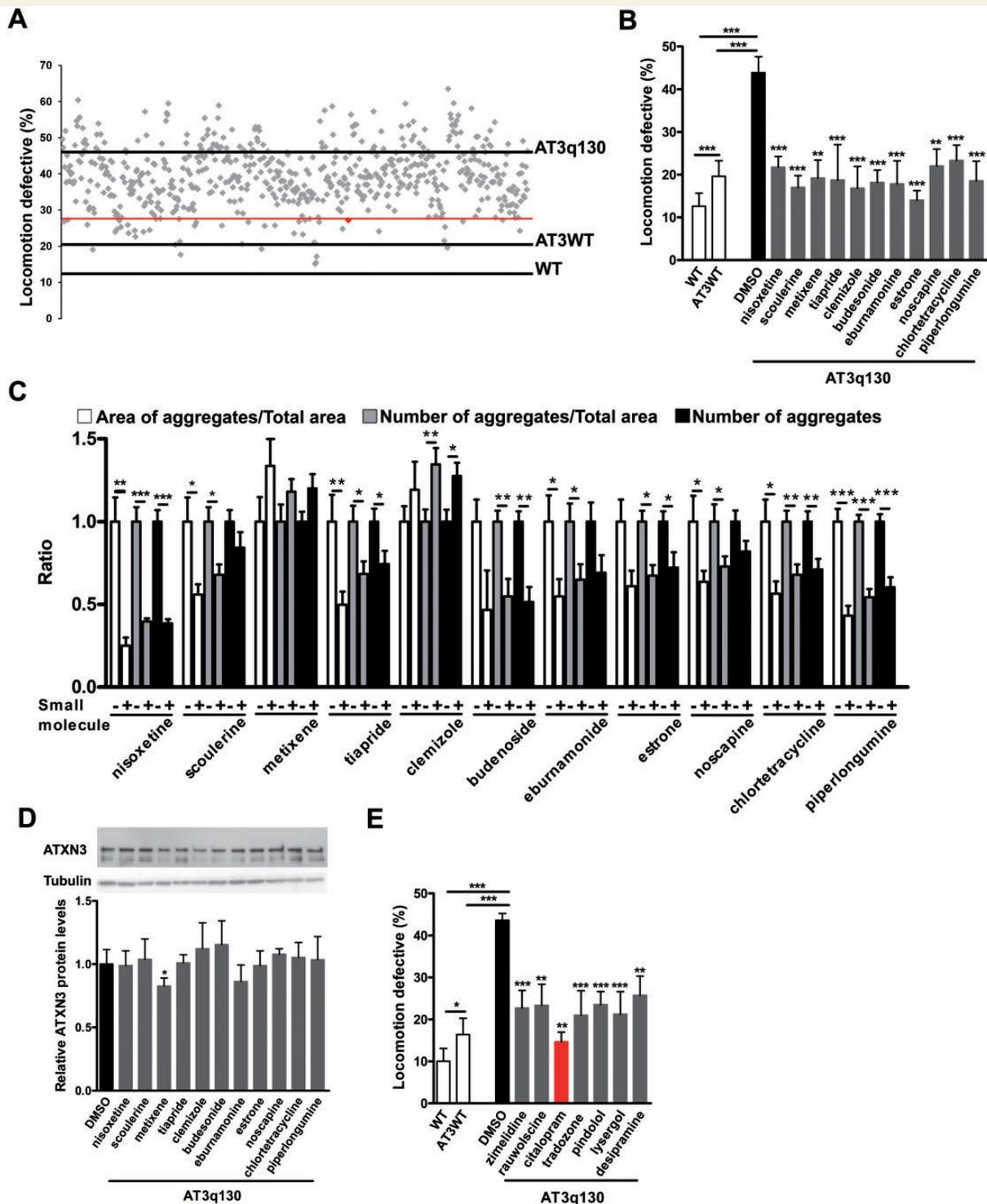
Figure 1 Identification of small-molecule suppressors of ATXN3 pathogenesis. (A) Graphical representation of the results of the *C. elegans*-based screening in which we assessed a subset of 599 compounds of the Prestwick Chemical library. Black lines represent the mean percentage of animals with locomotion impairment for untreated AT3q130, AT3WT and wild-type animals. Grey dots show the mean of percentage of locomotion impaired AT3q130 animals upon treatment for each compound. The red line represents the assay cut-off to a minimum of 50% of effect in animals' motor behaviour. The red dot represents the percentage of locomotion impaired AT3q130 animals upon citalopram treatment, as obtained in the primary screen. **(B)** Motility analysis of AT3q130 animals treated with the top 11 hit compounds found in the screen ($n = 4$, $\pm$ SD), **$P < 0.01$, ***$P < 0.001$ (Student's t-test). **(C)** Quantification of AT3q130 aggregation by confocal imaging and fluorescence intensity ($n \geqslant 10$, $\pm$ SD) *$P < 0.05$, **$P < 0.01$, ***$P < 0.001$ (ANOVA, Bonferroni's test). **(D)** Human ATXN3 expression in AT3q130 animals treated with the top hit compounds ($n = 4$–$6 \pm$ SEM). *$P < 0.05$ (Student's t-test). **(E)** Motility analysis of AT3q130 animals treated with compounds targeting serotonergic neurotransmission found in the screen ($n = 4$, $\pm$ SD), *$P < 0.05$, **$P < 0.01$, ***$P < 0.001$ (Student's t-test). WT = wild-type; AT3WT = wild-type ATXN3 expressing animals; AT3q130 = mutant ATXN3 expressing animals.

Table 1 Small molecule suppressors of ATXN3 pathogenesis grouped by their pharmacological action

| Cluster	Pharmacological action	Drug	Structure	Number of hit compounds
1	Neurotransmitter Adrenergic	Nisoxetine HCl	Propylamine	8
2	Neurotransmitter Serotonergic	Scoulerine	Alkaloid	8
3	Neurotransmitter Cholinergic	Metixene HCl	Heterocyclic	2
4	Neurotransmitter Dopaminergic	Tiapride HCl	Benzamide	2
5	Neurotransmitter Histaminergic	Clemizole HCl	Heterocyclic	3
6	Anti-inflammatory	Budesonide	Steroid	5
7	Cardiovascular	Eburnamonine	Alkaloid	5
8	Hormones/Hormone substituents	Estrone	Steroid	4
9	Analgesic	Noscapine	Alkaloid	2
10	Anti-infective	Chlortetracycline HCl	Polycyclic	8
11	Etc.	Piperlongumine	Heterocyclic	9
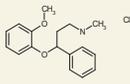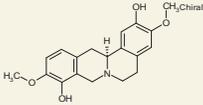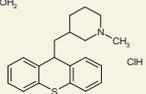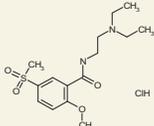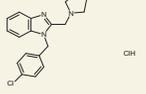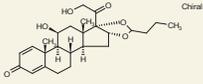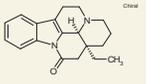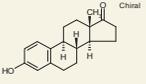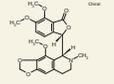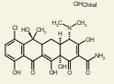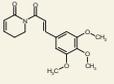
*HCl = hydrochloride.
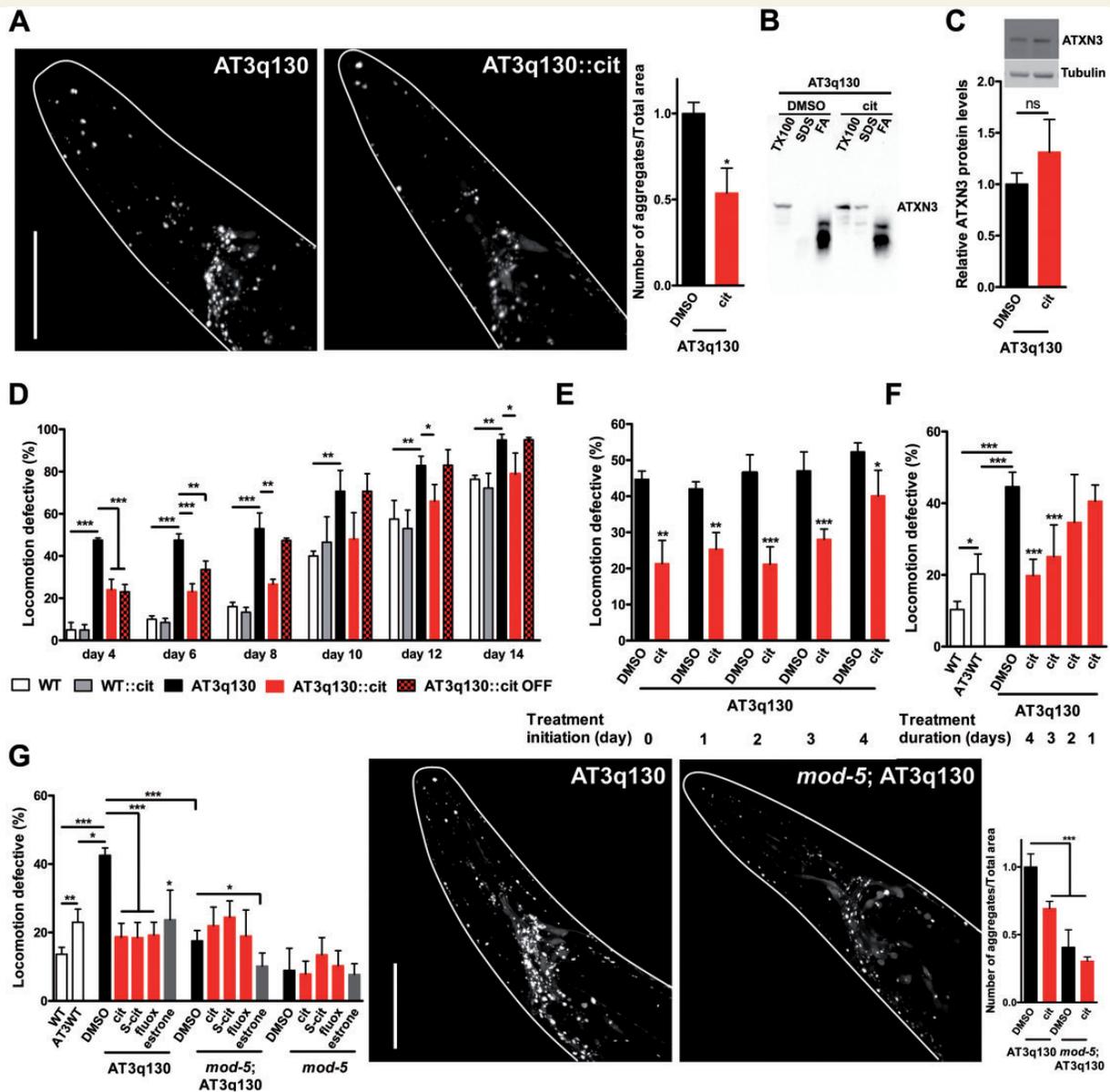
Figure 2 Early life chronic citalopram treatment suppressed mutant ATXN3 aggregation and neuronal dysfunction in *C. elegans*. (**A**) Aggregate quantification in AT3q130 animals upon citalopram (cit) treatment. (**B**) Representative western blot analysis of ATXN3 protein upon biochemical fractionation of AT3q130 protein extracts (out of *n* = 3). (**C**) Human ATXN3 protein levels in AT3q130 cit animals. (**D**) Motility of citalopram-treated wild-type (WT::cit) and AT3q130 (AT3q130::cit) animals and OFF-drug effect (AT3q130::cit OFF) as disease progressed. (**E**) Motor behaviour of AT3q130 cit animals treated for 4 days, with treatment initiation at the indicated days and (**F**) treatment duration for the indicated days. (**G**) Locomotion impairment and aggregation load of AT3q130 animals in the *mod-5* background and upon treatment with citalopram, S-citalopram and fluoxetine. For motor behaviour assays: ($n = 3$–$4 \pm$ SD), *$P < 0.05$, **$P < 0.01$, ***$P < 0.001$ (Student's *t*-test). For aggregate quantification: ($n \geqslant 8 \pm$ SD), *$P < 0.05$, **$P < 0.01$, ***$P < 0.001$ (ANOVA, Bonferroni's test). For western blot: ($n = 4 \pm$ SD), $P > 0.05$ (Student's *t*-test). TX100 = Triton™ X-100; FA = formic acid; cit = citalopram; S-cit = S-citalopram; fluox = fluoxetine; WT = wild-type.

Citalopram treatment improves motor balance and coordination of CMVMJD135 mice

To further investigate the therapeutic potential of citalopram, we used a transgenic mouse model of Machado-Joseph disease, CMVMJD135, that displays progressive Machado-Joseph disease-like motor decline and neuropathology, including ATXN3-positive intranuclear inclusions in the CNS (Silva-Fernandes *et al.*, 2014). Although CMVMJD135 mice showed no changes in baseline 5-HT levels measured by HPLC (Fig. 4), oral administration of citalopram (8 mg/kg) to these animals (study design; Fig. 5A) prevented their decreased body weight gain (Fig. 5B) and had significant beneficial effects on the motor phenotype. While there was only marginal
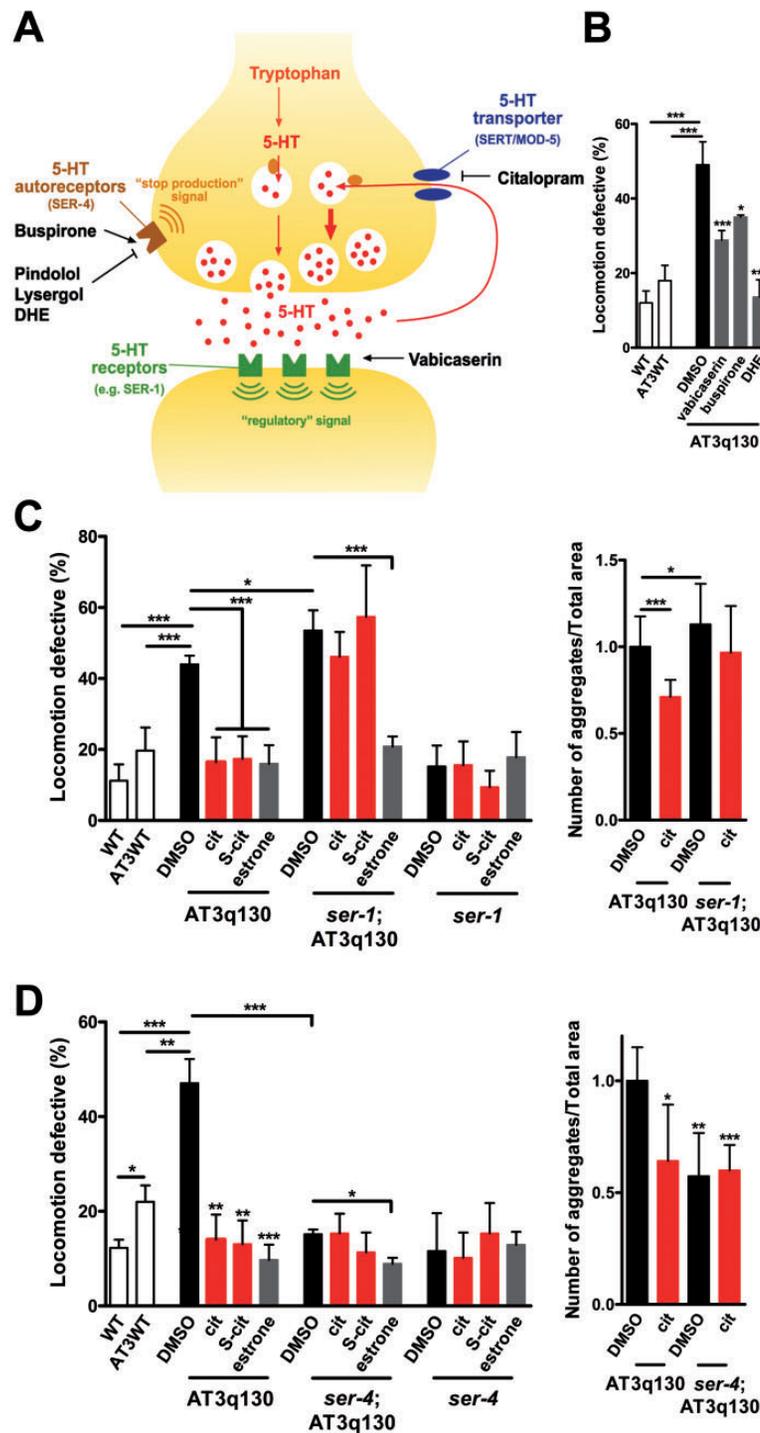
Figure 3 Serotonergic signalling improves ATXN3 pathogenesis in a G-protein coupled receptor-dependent manner. (A) Schematic of a serotonergic synapse showing that 5-HT is synthesized and released into the synaptic cleft, where it activates postsynaptic 5-HT receptors. Vabicaserin may activate the regulatory signalling coupled with SER-1. Pindolol, lysergol and DHE probably antagonize the 5-HT autoreceptor SER-4, whereas the 5-HT1A receptor agonist buspirone may desensitize the receptor, shutting down the stop production signal mediated by 5-HT autoreceptors in presynaptic neurons. **(B)** Motor behaviour of AT3q130 animals treated with vabicaserin, buspirone and dihydroergotamine. **(C)** Motility defects and aggregation load of AT3q130 animals in a *ser-1* genetic background, with and without cit, S-citalopram and estrone treatments. **(D)** Motility performance and mutant ATXN3 aggregation phenotypes of AT3q130 animals in the absence of SER-4. For motor behaviour assays: ($n = 3–4$, $\pm$ SD), $*P < 0.05$, $**P < 0.01$, $***P < 0.001$ (Student's *t*-test). For aggregate quantification: ($n \geqslant 12$, $\pm$ SD) $*P < 0.05$, $**P < 0.01$, $***P < 0.001$ (ANOVA, Bonferroni's test). DHE = dihydroergotamine; DMSO = dimethyl sulphoxide; cit = citalopram; S-cit = S-citalopram; fluox = fluoxetine.
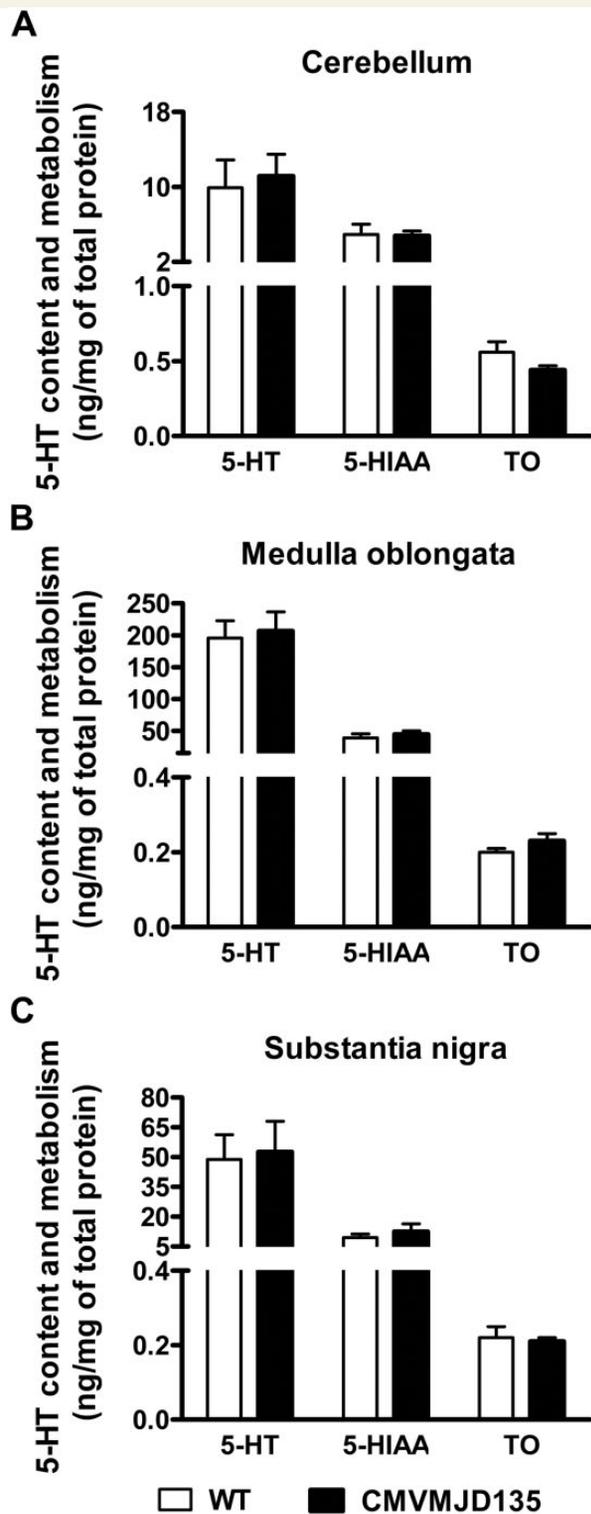
Figure 4 CMVMJD135 mice show normal levels of 5-HT and 5-HT metabolic turn over at fully symptomatic stages of disease. Levels of 5-HT, 5-HIAA and 5-HT turnover (5-HIAA/5-HT) were measured by HPLC (**A**) in the cerebellum ($n = 5$ wild-type; $n = 7$ CMVMJD135), (**B**) medulla oblongata ($n = 6$ wild-type; $n = 8$ CMVMJD135) and (**C**) substantia nigra ($n = 5$ wild-type; $n = 5$ CMVMJD135) at 24 weeks of age. Data presented as the mean $\pm$ SEM. $P > 0.05$ (Student's t-test). TO = turnover; WT = wild-type.

improvement in the dragging of the paws (Supplementary Fig. 5A) and limited effects on exploratory activity (Supplementary Fig. 5B), grip strength (Supplementary Fig. 5C) and hindlimb tonus (Supplementary Fig. 5D), citalopram treatment restored stride length to wild-type levels at advanced stages of the trial (Fig. 5C). Moreover, treated animals showed reduced tremors (Fig. 5D), reduced limb clasping (Fig. 5E), and improved gait quality (Fig. 5F). Citalopram treatment also resulted in a striking improvement in balance and motor coordination as compared to vehicle-treated CMVMJD135 mice. In the balance beam walk test, we observed major improvements in the 12 mm square beam from 20 to 34 weeks of age (Fig. 6A and Supplementary Video 1) and also in a wider (17 mm) round beam (Supplementary Fig. 5E). The most remarkable benefits of citalopram were observed in the motor swimming test (Fig. 6B), since at many time points and until quite late in the trial citalopram treated animals were indistinguishable from wild-type (Supplementary Video 2). Overall, these results demonstrate that citalopram can reduce the impairment in motor coordination of the Machado-Joseph disease mouse, with less benefit on strength, suggesting effects at the level of the brainstem, midbrain or cerebellum, rather than on spinocerebellar tracts and muscle innervation. Treatment also significantly delayed disease progression in mice.

Citalopram treated wild-type mice behaved similarly to their untreated littermates, confirming the specificity of the effect (Supplementary Fig. 6). Moreover, CMVMJD135 mice treated with a dosage of 13 mg/kg showed more limited improvements when compared to vehicle-treated controls in all paradigms mentioned above (Supplementary Fig. 7).

The analysis of brain tissue from CMVMJD135 mice showed that citalopram treatment (8 mg/kg) mitigated reactive astrogliosis (Fig. 6C) and decreased ATXN3 intranuclear inclusions in the brainstem (Fig. 6D), analogous to the reduction of neuronal aggregates in *C. elegans*. This reduction was observed in the pontine nuclei, reticulotegmental nuclei of pons and facial motor nuclei of CMVMJD135-treated mice when compared to their vehicle-treated counterparts (Fig. 6D); the impact of citalopram was less marked in the lateral reticular nuclei. This reduced ATXN3 aggregation did not correspond to lower levels of ATXN3 protein levels in the brainstem (Fig. 6E), suggesting that the effect of citalopram in mice is similar to that in *C. elegans*, affecting folding and stability of ATXN3 rather than clearance of the mutant protein. Citalopram treatment also had neuroprotective effects, rescuing loss of ChAT-positive motor neurons in the facial motor nuclei (Fig. 7A). The same trend was observed for motor neurons of the ventral horn of the lumbar spinal cord (Fig. 7B), albeit without statistical significance, in agreement with the observed phenotypic effects upon treatment. The mild reduction in Calbindin D28-K-positive cells seen in the cerebellar cortex of CMVMJD135 mice was also circumvented by citalopram treatment (Fig. 7C).
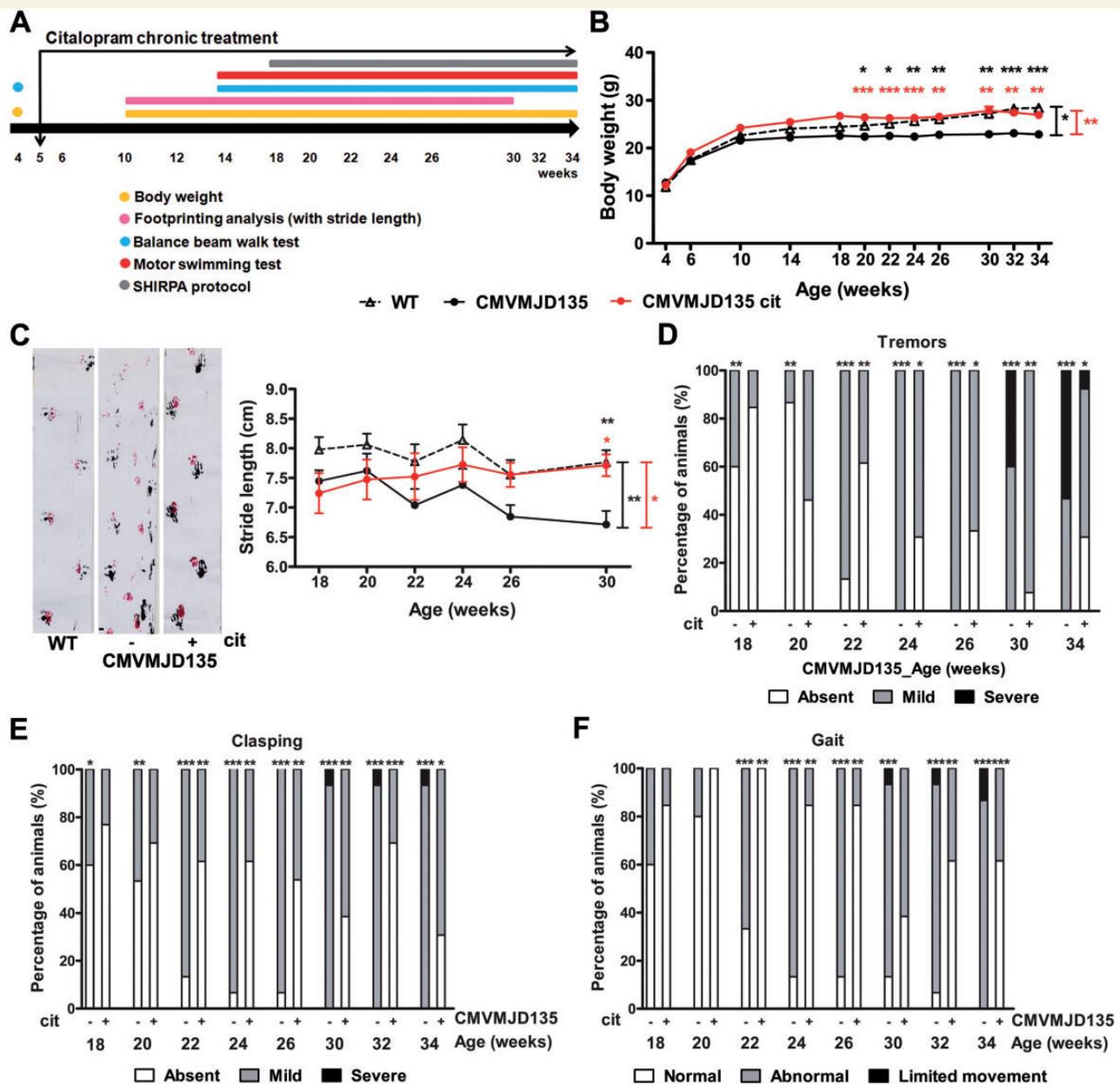
Figure 5 Impact of citalopram treatment at 8 mg/kg on the neurological deficits of CMVMJD135 mice. (**A**) Schematic representation of the preclinical therapeutic trial. Significant differences observed between vehicle (*n* = 13) and citalopram-treated CMVMJD135 mice (*n* = 16) in (**B**) body weight (*P* = 0.001, 20–34 weeks) and (**C**) stride length (*P* = 0.015, 30 weeks). (**D**) Tremors, (**E**) limb clasping and (**F**) gait were evaluated from 18 to 34 weeks of age with phenotype amelioration from 22 to 34 weeks of age. (*n* = 13–16, ± SD), *$P < 0.05$, **$P < 0.01$ and ***$P < 0.001$ (Mann-Whitney U-test for non-parametric variables and ANOVA, Tukey correction for continuous variables). cit = citalopram.

Discussion

In this study we describe a small molecule screen using a collection of FDA/EMA-approved drugs to identify modulators of neuronal dysfunction in transgenic *C. elegans* expressing mutant ATXN3. By using two model systems, we combined the ease and speed of screening in *C. elegans*, the ability to use genetics and selected small molecule agonists and antagonists of receptors and transporters to validate pathways, and the relevance of subsequent confirmation

in a vertebrate model of Machado-Joseph disease. This led to the identification of neuroactive compounds, among which modulators of the serotonergic pathway that strongly suppressed Machado-Joseph disease pathogenesis *in vivo*. In support of this screening strategy, many of the suppressors of ATXN3 pathogenesis identified in our study have been shown to be effective in other neurodegenerative disorders, including Parkinson's and Alzheimer's disease, and also in Machado-Joseph disease (Clarke *et al.*, 1966; Perenyi *et al.*, 1985; Kanai *et al.*,
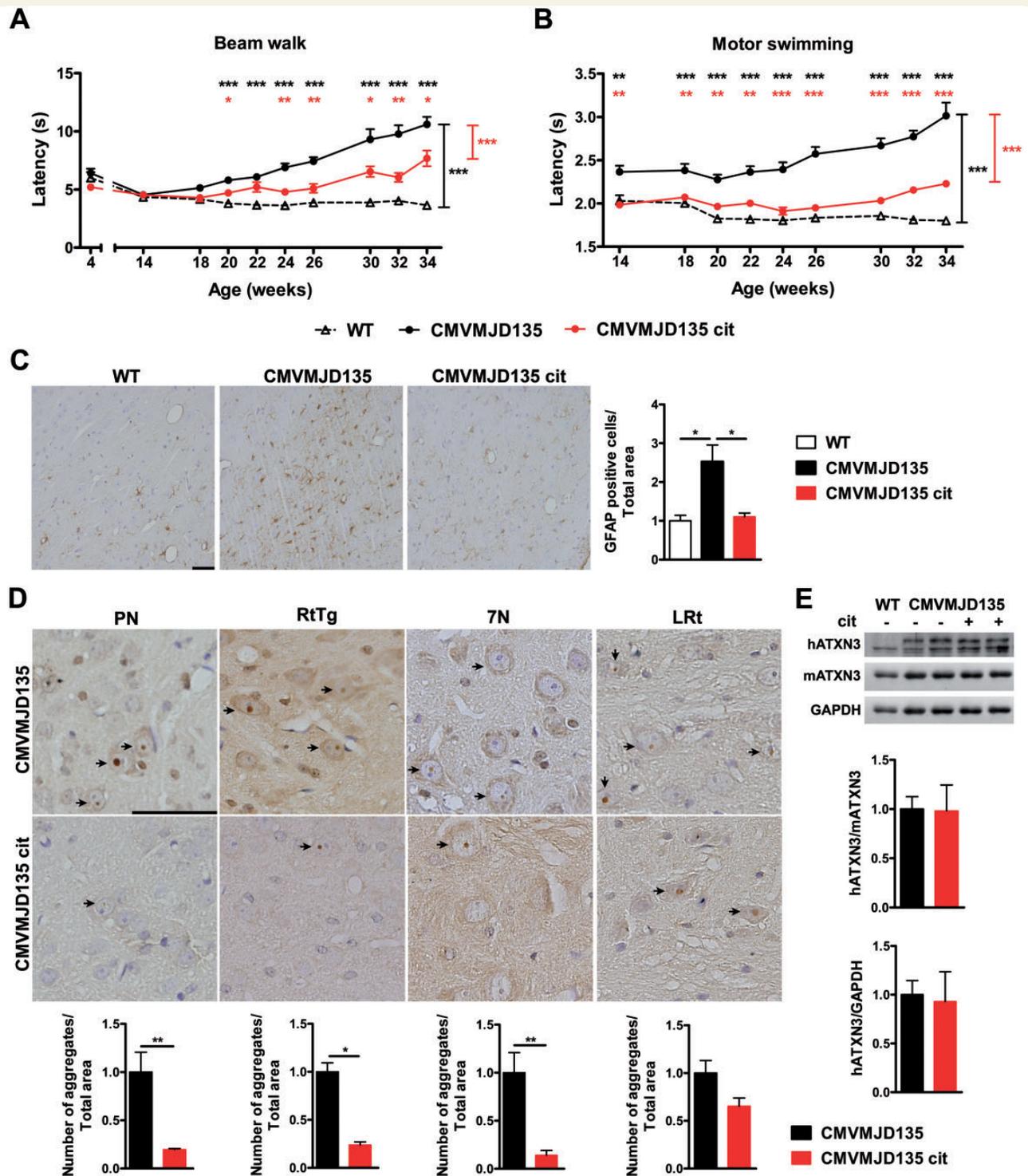
Figure 6 Citalopram treatment ameliorates balance and motor coordination and suppresses mutant ATXN3 aggregation in Machado-Joseph disease mice. Significant differences observed between vehicle ($n = 13$) and citalopram-treated CMVMJD135 mice ($n = 16$) in the (**A**) square beam ($P < 0.001$, 20–34 weeks) and (**B**) motor swimming ($P < 0.001$, 14–34 weeks) tests. (**C**) Immunohistochemistry and quantification of GFAP-positive cells per area in substantia nigra from wild-type, vehicle- and citalopram-treated CMVMJD135 mice ($n = 5$ per group, 34 weeks). (**D**) Neuronal inclusions in the pontine nuclei, reticulotegmental nucleus of the pons, facial motor nucleus and lateral reticular nucleus of vehicle and citalopram-treated CMVMJD135 mice ($n = 4$, 34 weeks). (**E**) Brainstem immunoblots and quantification of total human ATXN3 protein from vehicle and citalopram-treated CMVMJD135 mice ($n = 5$, 34 weeks). Data presented as mean ± SEM, *$P < 0.05$ and **$P < 0.01$ [ANOVA, Tukey correction (**A** and **B**) and one-way ANOVA (**C–E**)]. Scale bars = 20 μm. cit = citalopram; WT = wild-type; SN = substantia nigra; PN = pontine nuclei; RtTg = reticulotegmental nuclei of pons; 7N = facial motor nuclei; LRt = lateral reticular nuclei.

Figure 7 Citalopram treatment shows neuroprotective effects in CMVMJD135 mice. (**A**) Immunohistochemistry and quantification of ChAT-positive cells per total area in the facial motor nucleus from wild-type, vehicle and citalopram-treated CMVMJD135 mice (*n* = 4 per group, 34 weeks). (**B**) Immunohistochemistry and quantification of ChAT-positive cells per total area in the lumbar region of the ventral horn of the spinal cord (LSC) from wild-type, vehicle and citalopram-treated CMVMJD135 mice (*n* = 3–4 per group, 34 weeks). (**C**) Immunohistochemistry and quantification of Calbindin D28K-positive Purkinje cells per total area in the cerebellar cortex from wild-type, vehicle and citalopram-treated CMVMJD135 mice (*n* = 4 per group, 34 weeks). Data presented as mean ± SEM, *$P < 0.05$ and **$P < 0.01$ (one-way ANOVA). Scale bars = 200 μm (**A**) and 100 μm (**B** and **C**). cit = citalopram; WT = wild-type; 7N = facial motor nuclei; LSC = lumbar spinal cord; CBX = cerebellar cortex.

2003; Cho *et al.*, 2009; Cirrito *et al.*, 2011). A more in-depth understanding of the mechanism of action of these suppressors of expanded ATXN3 toxicity and their ability to modulate aggregation offers new opportunities for small-molecule therapeutics for Machado-Joseph disease and other protein conformational diseases.

Citalopram and other SSRIs suppressed Machado-Joseph disease pathogenesis in the *C. elegans* and mouse models, showing beneficial effects on motility/coordination, aggregation of mutant ATXN3, and disease progression. MOD-5 (and SERT) inhibition by citalopram likely results in increased extracellular 5-HT levels and enhanced serotonergic neurotransmission that can elicit 5-HT dependent effects on neuronal activities, adaptation (Blier and de Montigny, 1999; El Mansari *et al.*, 2005; Schilstrom *et al.*, 2011), and remodelling (Musazzi *et al.*, 2010;

Bessa *et al.*, 2013). Indeed, ablation of the postsynaptic receptor SER-1 (Hamdan *et al.*, 1999), which is pharmacologically similar to the mammalian 5-HT2 receptor, aggravated ATXN3 pathogenesis. The beneficial action of citalopram required SER-1, suggesting that the downstream effects of this drug are mediated by signalling cascades involving this receptor. Furthermore, ablation of SER-4, which shares similarity to vertebrates' 5-HT1 autoreceptors, rescued motor neuron dysfunction and reduced ATXN3 aggregation *in vivo*.

The therapeutic effects of SSRIs for amelioration of mutant ATXN3-mediated neurotoxicity in both *C. elegans* and mice required chronic treatment; likewise, citalopram prolonged treatment is necessary in depression (Blier and de Montigny, 1999). Such SSRI treatment modalities result in 5-HT1A autoreceptor desensitization (Blier and De

Montigny, 1983; Lanfumey *et al.*, 2008), which inactivates the negative feedback mechanism taking place in presynaptic neurons, thereby increasing 5-HT availability and activating postsynaptic receptors (Lanfumey and Hamon, 2004). Pindolol, a β-adrenergic receptor partial agonist with 5-HT1A receptor antagonist properties, when combined with SSRIs, results in a significant decrease in time to first response compared with SSRIs alone. Moreover, a faster desensitization of 5-HT1A autoreceptors by a direct agonist (e.g. buspirone) may also accelerate the therapeutic efficacy of SSRIs (Blier and Ward, 2003). Consistently, targeting 5-HT autoreceptors by chronic treatment ameliorated mutant ATXN3-mediated pathogenesis in *C. elegans*. Serotonin receptors in nematodes and mammalians, while homologous, may not be functionally identical (Komuniecki *et al.*, 2004); therefore, it would be important to identify the specific 5-HT receptors required for citalopram's effect on toxicity and aggregation of mutant ATXN3 in mice.

In Huntingdon's disease mouse models, SSRI treatment resulted in striatal and memory preservation and extended survival (Lauterbach, 2013). Citalopram has also been shown to be beneficial in models of Alzheimer's disease and in healthy human volunteers by reducing amyloid-β in the CSF (Cirrito *et al.*, 2011; Sheline *et al.*, 2014). The need for chronic and early symptomatic treatment in Machado-Joseph disease suggests a neuroprotective mechanism rather than immediate effects on signalling cascades (Sheline *et al.*, 2014) or correction of an imbalance of 5-HT in Machado-Joseph disease mice. Moreover, the effect of citalopram and MOD-5 inactivation on aggregation ATXN3 is consistent with an impact of serotonergic neurotransmission on the rebalance of proteostasis state of the organism. Indeed, it has been recently described that the release of serotonin from neurons signals to distal tissues the activation of protective mechanisms to prevent proteotoxicity (Tatum *et al.*, 2015).

Comparing the effects obtained with citalopram with those described in the literature for other molecules with positive effect in Machado-Joseph disease models, this SSRI appears to have a higher therapeutic efficacy. From our own work, when we compare the current results with the previous findings for the Hsp90 inhibitor 17-DMAG (Silva-Fernandes *et al.*, 2014), we observe a more pronounced therapeutic effect of citalopram. Namely, the manifestation of motor swimming defects was delayed 8 weeks by 17-DMAG treatment versus at least 20 weeks by citalopram treatment; also, at 30 weeks, the percentage of effect of 17-DMAG in this test was 33%, and that of citalopram was 79%. The difference in performance between the treated groups (normalized to the respective non-treated groups) in the two experiments was statistically significant at this age ($P = 0.018$).

In conclusion, the efficacy of citalopram in suppression of ATXN3 pathogenesis in two disease models, as well as its safety record of being widely used in depression patients, prompts us to suggest this drug for clinical trials in patients with Machado-Joseph disease.

Acknowledgements

Funding

Supplementary material

Supplementary material is available at *Brain* online.

References

Balch WE, Morimoto RI, Dillin A, Kelly JW. Adapting proteostasis for disease intervention. Science 2008; 319: 916–9.

Bessa JM, Morais M, Marques F, Pinto L, Palha JA, Almeida OF, et al. Stress-induced anhedonia is associated with hypertrophy of medium spiny neurons of the nucleus accumbens. Transl Psychiatry 2013; 3: e266.

Blakely RD, De Felice LJ, Hartzell HC. Molecular physiology of norepinephrine and serotonin transporters. J Exp Biol 1994; 196: 263–81.

Blier P, De Montigny C. Electrophysiological investigations on the effect of repeated zimelidine administration on serotonergic neurotransmission in the rat. J Neurosci 1983; 3: 1270–8.

Blier P, de Montigny C. Serotonin and drug-induced therapeutic responses in major depression, obsessive-compulsive and panic disorders. Neuropsychopharmacology 1999; 21 (2 Suppl): 91S–8S.

Blier P, Ward NM. Is there a role for 5-HT1A agonists in the treatment of depression? Biol Psychiatry 2003; 53: 193–203.

Brenner S. The genetics of Caenorhabditis elegans. Genetics 1974; 77: 71–94.

Chen X, Tang TS, Tu H, Nelson O, Pook M, Hammer R, et al. Deranged calcium signaling and neurodegeneration in spinocerebellar ataxia type 3. J Neurosci 2008; 28: 12713–24.

Cho Y, Son HJ, Kim EM, Choi JH, Kim ST, Ji IJ, et al. Doxycycline is neuroprotective against nigral dopaminergic degeneration by a dual mechanism involving MMP-3. Neurotox Res 2009; 16: 361–71.

Chong CR, Sullivan DJ, Jr. New uses for old drugs. Nature 2007; 448: 645–6.

Chou AH, Chen SY, Yeh TH, Weng YH, Wang HL. HDAC inhibitor sodium butyrate reverses transcriptional downregulation and ameliorates ataxic symptoms in a transgenic mouse model of SCA3. Neurobiol Dis 2011; 41: 481–8.

Cirrito JR, Disabato BM, Restivo JL, Verges DK, Goebel WD, Sathyan A, et al. Serotonin signaling is associated with lower amyloid-beta levels and plaques in transgenic mice and humans. Proc Natl Acad Sci USA 2011; 108: 14968–73.

Clarke S, Hay GA, Vas CJ. Therapeutic action of methixene hydrochloride on Parkinsonian tremor and a description of a new tremor-recording transducer. Br J Pharmacol Chemother 1966; 26: 345–50.

Corradetti R, Laaris N, Hanoun N, Laporte AM, Le Poul E, Hamon M, et al. Antagonist properties of (-)-pindolol and WAY 100635 at somatodendritic and postsynaptic 5-HT1A receptors in the rat brain. Br J Pharmacol 1998; 123: 449–62.

Costa Mdo C, Luna-Cancalon K, Fischer S, Ashraf NS, Ouyang M, Dharia RM, et al. Toward RNAi therapy for the polyglutamine disease Machado-Joseph disease. Mol Ther 2013; 21: 1898–908.

Coutinho P, Andrade C. Autosomal dominant system degeneration in Portuguese families of the Azores Islands. A new genetic disorder involving cerebellar, pyramidal, extrapyramidal and spinal cord motor functions. Neurology 1978; 28: 703–9.

Cushman-Nick M, Bonini NM, Shorter J. Hsp104 suppresses polyglutamine-induced degeneration post onset in a drosophila MJD/SCA3 model. PLoS Genet 2013; 9: e1003781.

D'Abreu A, Franca MC, Jr, Paulson HL, Lopes-Cendes I. Caring for Machado-Joseph disease: current understanding and how to help patients. Parkinsonism Relat Disord 2010; 16: 2–7.

Dunlop J, Watts SW, Barrett JE, Coupet J, Harrison B, Mazandarani H, et al. Characterization of vabicaserin (SCA-136), a selective 5-hydroxytryptamine 2C receptor agonist. J Pharmacol Exp Ther 2011; 337: 673–80.

El Mansari M, Sanchez C, Chouvet G, Renaud B, Haddjeri N. Effects of acute and long-term administration of escitalopram and citalopram on serotonin neurotransmission: an in vivo electrophysiological study in rat brain. Neuropsychopharmacology 2005; 30: 1269–77.

Gidalevitz T, Ben-Zvi A, Ho KH, Brignull HR, Morimoto RI. Progressive disruption of cellular protein folding in models of polyglutamine diseases. Science 2006; 311: 1471–4.

Gidalevitz T, Krupinski T, Garcia S, Morimoto RI. Destabilizing protein polymorphisms in the genetic background direct phenotypic expression of mutant SOD1 toxicity. PLoS Genet 2009; 5: e1000399.

Hamdan FF, Ungrin MD, Abramovitz M, Ribeiro P. Characterization of a novel serotonin receptor from Caenorhabditis elegans: cloning and expression of two splice variants. J Neurochem 1999; 72: 1372–83.

Kaletta T, Hengartner MO. Finding function in novel targets: C. elegans as a model organism. Nat Rev Drug Discov 2006; 5: 387–98.

Kanai K, Kuwabara S, Arai K, Sung JY, Ogawara K, Hattori T. Muscle cramp in Machado-Joseph disease: altered motor axonal excitability properties and mexiletine treatment. Brain 2003; 126 (Pt 4): 965–73.

Kawaguchi Y, Okamoto T, Taniwaki M, Aizawa M, Inoue M, Katayama S, et al. CAG expansions in a novel gene for Machado-Joseph disease at chromosome 14q32.1. Nat Genet 1994; 8: 221–8.

Koch P, Breuer P, Peitz M, Jungverdorben J, Kesavan J, Poppe D, et al. Excitation-induced ataxin-3 aggregation in neurons from patients with Machado-Joseph disease. Nature 2011; 480: 543–6.

Komuniecki RW, Hobson RJ, Rex EB, Hapiak VM, Komuniecki PR. Biogenic amine receptors in parasitic nematodes: what can be learned from Caenorhabditis elegans? Mol Biochem Parasitol 2004; 137: 1–11.

Lanfumey L, Hamon M. 5-HT1 receptors. Curr Drug Targets CNS Neurol Disord 2004; 3: 1–10.

Lanfumey L, Mongeau R, Cohen-Salmon C, Hamon M. Corticosteroid-serotonin interactions in the neurobiological mechanisms of stress-related disorders. Neurosci Biobehav Rev 2008; 32: 1174–84.

Lauterbach EC. Neuroprotective effects of psychotropic drugs in Huntington's disease. Int J Mol Sci 2013; 14: 22558–603.

Mandrioli R, Mercolini L, Saracino MA, Raggi MA. Selective serotonin reuptake inhibitors (SSRIs): therapeutic drug monitoring and pharmacological interactions. Curr Med Chem 2012; 19: 1846–63.

Menzies FM, Huebener J, Renna M, Bonin M, Riess O, Rubinsztein DC. Autophagy induction reduces mutant ataxin-3 levels and toxicity in a mouse model of spinocerebellar ataxia type 3. Brain 2010; 133(Pt 1): 93–104.

Morimoto RI. Proteotoxic stress and inducible chaperone networks in neurodegenerative disease and aging. Genes Dev 2008; 22: 1427–38.

Morley JF, Morimoto RI. Regulation of longevity in Caenorhabditis elegans by heat shock factor and molecular chaperones. Mol Biol Cell 2004; 15: 657–64.

Musazzi L, Mallei A, Tardito D, Gruber SH, El Khoury A, Racagni G, et al. Early-life stress and antidepressant treatment involve synaptic signaling and Erk kinases in a gene-environment model of depression. J Psychiatr Res 2010; 44: 511–20.

Nascimento-Ferreira I, Nobrega C, Vasconcelos-Ferreira A, Onofre I, Albuquerque D, Aveleira C, et al. Beclin 1 mitigates motor and neuropathological deficits in genetic mouse models of Machado-Joseph disease. Brain 2013; 136 (Pt 7): 2173–88.

Nobrega C, Nascimento-Ferreira I, Onofre I, Albuquerque D, Hirai H, Deglon N, et al. Silencing mutant ataxin-3 rescues motor deficits and neuropathology in Machado-Joseph disease transgenic mice. PLoS One 2013; 8: e52396.

Nussbaum-Krammer CI, Park KW, Li L, Melki R, Morimoto RI. Spreading of a prion domain from cell-to-cell by vesicular transport in Caenorhabditis elegans. PLoS Genet 2013; 9: e1003351.

Olde B, McCombie WR. Molecular cloning and functional expression of a serotonin receptor from Caenorhabditis elegans. J Mol Neurosci 1997; 8: 53–62.

Pain and distress in laboratory rodents and lagomorphs. Report of the Federation of European Laboratory Animal Science Associations (FELASA) Working Group on Pain and Distress accepted by the FELASA Board of Management November 1992. Lab Anim 1994; 28: 97–112.

Perenyi A, Arato M, Bagdy G, Frecska E, Szucs R. Tiapride in the treatment of tardive dyskinesia: a clinical and biochemical study. J Clin Psychiatry 1985; 46: 229–31.

Pertz HH, Brown AM, Gager TL, Kaumann AJ. Simple O-acylated derivatives of lysergol and dihydrolysergol-I: synthesis and interaction with 5-HT2A, 5-HT2C and 5-HT1B receptors, and alpha1 adrenergic receptors. J Pharm Pharmacol 1999; 51: 319–30.

Ranganathan R, Sawin ER, Trent C, Horvitz HR. Mutations in the Caenorhabditis elegans serotonin reuptake transporter MOD-5 reveal serotonin-dependent and -independent activities of fluoxetine. J Neurosci 2001; 21: 5871–84.

Robertson AL, Headey SJ, Saunders HM, Ecroyd H, Scanlon MJ, Carver JA, et al. Small heat-shock proteins interact with a flanking

domain to suppress polyglutamine aggregation. Proc Natl Acad Sci USA 2010; 107: 10424–9.

Ross CA, Margolis RL, Becher MW, Wood JD, Engelender S, Cooper JK, et al. Pathogenesis of neurodegenerative diseases associated with expanded glutamine repeats: new answers, new questions. Prog Brain Res 1998; 117: 397–419.

Santos M, Summavielle T, Teixeira-Castro A, Silva-Fernandes A, Duarte-Silva S, Marques F, et al. Monoamine deficits in the brain of methyl-CpG binding protein 2 null mice suggest the involvement of the cerebral cortex in early stages of Rett syndrome. Neuroscience 2010; 170: 453–67.

Schilstrom B, Konradsson-Geuken A, Ivanov V, Gertow J, Feltmann K, Marcus MM, et al. Effects of S-citalopram, citalopram, and R-citalopram on the firing patterns of dopamine neurons in the ventral tegmental area, N-methyl-D-aspartate receptor-mediated transmission in the medial prefrontal cortex and cognitive function in the rat. Synapse 2011; 65: 357–67.

Schols L, Bauer P, Schmidt T, Schulte T, Riess O. Autosomal dominant cerebellar ataxias: clinical features, genetics, and pathogenesis. Lancet Neurol 2004; 3: 291–304.

Sheline YI, West T, Yarasheski K, Swarm R, Jasielec MS, Fisher JR, et al. An antidepressant decreases CSF Abeta production in healthy individuals and in transgenic AD mice. Sci Transl Med 2014; 6: 236re4.

Shim JS, Liu JO. Recent Advances in Drug Repositioning for the Discovery of New Anticancer Drugs. Int J Biol Sci 2014; 10: 654–63.

Silva-Fernandes A, Costa Mdo C, Duarte-Silva S, Oliveira P, Botelho CM, Martins L, et al. Motor uncoordination and neuropathology in a transgenic mouse model of Machado-Joseph disease lacking intranuclear inclusions and ataxin-3 cleavage products. Neurobiol Dis 2010; 40: 163–76.

Silva-Fernandes A, Duarte-Silva S, Neves-Carvalho A, Amorim M, Soares-Cunha C, Oliveira P, et al. Chronic treatment with 17-DMAG improves balance and coordination in a new mouse model of Machado-Joseph disease. Neurotherapeutics 2014; 11: 433–49.

Takei A, Hamada T, Yabe I, Sasaki H. Treatment of cerebellar ataxia with 5-HT1A agonist. Cerebellum 2005; 4: 211–5.

Tatum MC, Ooi FK, Chikka MR, Chauve L, Martinez-Velazquez LA, Steinbush HWM, et al. Neuronal serotonin release triggers the heat shock response in C. elegans in the absence of temperature increase. Curr Biol 2015; 52: 163–74.

Teixeira-Castro A, Ailion M, Jalles A, Brignull HR, Vilaca JL, Dias N, et al. Neuron-specific proteotoxicity of mutant ataxin-3 in C. elegans: rescue by the DAF-16 and HSF-1 pathways. Hum Mol Genet 2011a; 20: 2996–3009.

Teixeira-Castro A, Dias N, Rodrigues P, Oliveira JF, Rodrigues NF, Maciel P, et al. An image processing application for quantification of protein aggregates in Caenorhabditis elegans. In: Rocha MP, Corchado JM, Fdez Riverola F, Valencia A, editors. Advances 55 in Intelligent and Soft Computing Series. Vol. 93. Springer-Verlag; 2011b. (ISBN 978-3-642-19913-4).

Villalon CM, Centurion D, Valdivia LF, de Vries P, Saxena PR. Migraine: pathophysiology, pharmacology, treatment and future trends. Curr Vasc Pharmacol 2003; 1: 71–84.

Voisine C, Varma H, Walker N, Bates EA, Stockwell BR, Hart AC. Identification of potential therapeutic drugs for huntington's disease using Caenorhabditis elegans. PLoS One 2007; 2: e504.

Warrick JM, Morabito LM, Bilen J, Gordesky-Gold B, Faust LZ, Paulson HL, et al. Ataxin-3 suppresses polyglutamine neurodegeneration in Drosophila by a ubiquitin-associated mechanism. Mol Cell 2005; 18: 37–48.